Self-Mode-Locking of Quantum Cascade Lasers with Giant Ultrafast Optical Nonlinearities

Roberto Paiella, *et al.*

Science **290**, 1739 (2000);
DOI: 10.1126/science.290.5497.1739

Science (print ISSN 0036-8075; online ISSN 1095-9203) is published weekly, except the last week in December, by the American Association for the Advancement of Science, 1200 New York Avenue NW, Washington, DC 20005.

Self–Mode-Locking of Quantum Cascade Lasers with Giant Ultrafast Optical Nonlinearities

Roberto Paiella,[1]* Federico Capasso,[1] Claire Gmachl,[1] Deborah L. Sivco,[1] James N. Baillargeon,[1] Albert L. Hutchinson,[1] Alfred Y. Cho,[1] H. C. Liu[2]

We report on the generation of picosecond self–mode-locked pulses from midinfrared quantum cascade lasers, at wavelengths within the important molecular fingerprint region. These devices are based on intersubband electron transitions in semiconductor nanostructures, which are characterized by some of the largest optical nonlinearities observed in nature and by picosecond relaxation lifetimes. Our results are interpreted with a model in which one of these nonlinearities, the intensity-dependent refractive index of the lasing transition, creates a nonlinear waveguide where the optical losses decrease with increasing intensity. This favors the generation of ultrashort pulses, because of their larger instantaneous intensity relative to continuous-wave emission.

Ever since the invention of the laser in 1960, an extensive research effort has focused on the development of ultrafast laser sources. Optical pulses with duration in the picosecond and femtosecond range have been generated in several gas and solid-state laser media, particularly at wavelengths ranging from the ultraviolet to the near infrared (*1*–*3*). The most common technique for ultrashort pulse generation is mode-locking, in which the longitudinal modes of the laser cavity are locked in phase, by some external or internal mechanism, to produce a train of pulses with repetition rate equal to the cavity roundtrip frequency. These sources have allowed for a marked improvement in the temporal resolution of a myriad of measurements in physics, chemistry, and biology. Commercial applications are also emerging in several fields (*2*), including medical diagnostics, material processing, and optical communications. On the other hand, the technologically important midinfrared spectrum (3 to 15 μm) still lacks compact and convenient laser sources of ultrashort pulses (*4*). This spectral region is known as the molecular fingerprint region, because many chemical and biological species have their telltale absorption features associated with molecular vibrations in this wavelength range. As a result, several applications exist for ultrafast midinfrared lasers, ranging from time-resolved spectroscopy to coherent control (*2*).

We report on the generation of picosecond self–mode-locked pulses of midinfrared radiation in quantum cascade (QC) lasers (*5*, *6*). These devices are based on intersubband electron transitions, i.e., transitions between quantized conduction-band states in semiconductor quantum wells. These transitions are characterized by some of the largest optical nonlinearities ever observed (*7*–*10*). Furthermore, intersubband carrier relaxation is controlled by an extremely fast (picosecond) mechanism, namely scattering by optical phonons. We emphasize that although large resonant nonlinearities are found in several other laser systems, their response is always much slower. Because of this unique combination of giant magnitude and ultrafast dynamics, intersubband optical nonlinearities have attracted considerable attention, and several applications to high-speed optoelectronic devices have been proposed (*7*–*11*). Here, we interpret our results in terms of self–mode-locking (SML) from one of these nonlinearities, the intensity-dependent refractive index [often referred to as the optical Kerr effect (*12*)] of the intersubband laser transition. Specifically, this nonlinearity consists of a refractive index n that varies with optical intensity I according to the approximate expression $n = n_0 + n_2 I$, where n_2 is the nonlinear refractive index.

Several QC lasers were used in this work, emitting at either 5- or 8-μm wavelength and similar to the devices described in (*13*) and (*14*), except for their unusually long waveguides (≳3.5 mm). The laser material was grown by molecular beam epitaxy in the InGaAs/AlInAs material system lattice matched to InP substrates. The individual devices were mounted inside a helium flow cryostat (*15*) and biased with a dc current. Over a wide range of dc bias, these lasers were found to emit an extremely broad (up to 1.5 THz, about 50% of the gain bandwidth) multimode spectrum, characterized by a smooth multipeaked envelope. A series of these spectra, measured with a Nicolet Fourier transform infrared spectrometer (FTIR), is shown (Fig. 1), for a 3.5-mm-long 8-μm QC laser at 80 K. At the same time, these devices were found to self-pulsate at their cavity roundtrip frequency. This was ascertained by detecting their output with a fast quantum-well infrared photodetector (QWIP) (*16*, *17*) and displaying the resulting photocurrent in a spectrum analyzer. A sharp feature centered at the laser roundtrip frequency (≃13 GHz in the device of Fig. 1) was observed, whose peak power corresponds to a modulation amplitude of the laser beam of the order (at least 20%) of the measured average optical power. This feature results from the mutual beating of adjacent modes in the optical spectrum. Its large magnitude, strong stability, and narrow width (typically less than 100 kHz) indicate negligible random drift of the modes' relative phases, as expected in a mode-locked laser. An example is shown in the inset of Fig. 1.

As a result of this phase locking, the amplitudes of the lasing modes add coherently to produce a periodic time-varying optical waveform. Information about the temporal characteristics of such mode-locked wave-

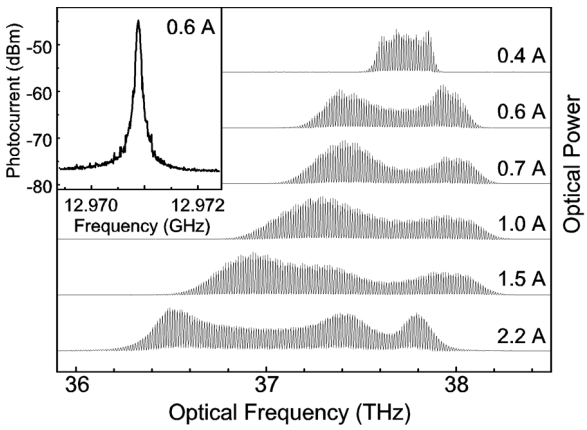

Fig. 1. Optical spectra of a 3.5-mm-long, 8-μm wavelength QC laser (from wafer D2396F) at a temperature of 80 K, under conditions of self–mode-locking, for different values of the laser dc bias current. (Inset) Microwave spectrum of the photocurrent generated by the same laser (at a bias of 0.6 A) in a high-speed quantum-well infrared photodetector (measured with a 1-kHz resolution bandwidth). As explained in the text, this peak indicates a large-signal modulation of the laser beam. A similar peak was also observed in the microwave spectrum of the QC laser current, measured through a high-speed bias "tee."

[1]Bell Laboratories, Lucent Technologies, 600 Mountain Avenue, Murray Hill, NJ 07974, USA. [2]Institute for Microstructural Sciences, National Research Council, Ottawa, Ontario, K1A 0R6, Canada.

*To whom correspondence should be addressed. E-mail: robertop@lucent.com

forms is traditionally obtained with second-order autocorrelation measurements. At present, however, these are not well developed in the midinfrared, especially at the relatively low power levels of these lasers. In any case, an indicative test of pulsed emission is provided by the linear autocorrelation traces generated by the FTIR. An example is shown for both an 8-μm (Fig. 2A) and a 5-μm (Fig. 2B) device. An FTIR is a Michelson interferometer (*18*) (Fig. 2C), and these autocorrelation traces consist of the interference fringes from the beams in the two interferometer arms. In the presence of ultrashort pulses, such fringes can only occur when pulses from the two arms temporally overlap on the detector. The result is an autocorrelation trace consisting of narrow spikes at delay times equal to multiples of the pulse separation time (*19*), which is exactly what is observed (Fig. 2). In particular, the negligible amplitude of the fringes between the spikes suggests that these lasers are indeed emitting a train of ultrashort pulses (*20*) with good modulation depth.

The multipeaked envelopes observed in the optical spectra of Fig. 1 are also consistent with pulsed emission and cannot otherwise be explained in terms of unlocked multimode emission, given the primarily homogeneously broadened narrow gain curves of these QC lasers (*14*). In particular, these structures are typical of short laser pulses undergoing strong self-phase modulation (*21*). Namely, in the presence of an intensity-dependent refractive index, the optical field develops a time-varying phase proportional to the pulse intensity profile (*12*). Correspondingly, the optical spectrum develops an oscillatory envelope and broadens to (*21*)

$$\Delta\omega_{rms} = \frac{\sqrt{2\log 2}}{\tau_p}\sqrt{1+\frac{4}{3\sqrt{3}}\phi_{max}^2} \qquad (1)$$

where $\Delta\omega_{rms}$ is the root-mean-square (rms) spectral width, τ_p is the pulse full-width-at-half-maximum (FWHM), and a Gaussian pulse shape is assumed. Finally, ϕ_{max} is the maximum nonlinear phase shift, given by

$$\phi_{max} = \frac{4\pi L}{\lambda}\Gamma n_2 I_{max} \qquad (2)$$

where L is the laser length, λ is the wavelength, Γ is the confinement factor (the fractional mode overlap with the QC active layers), n_2 is the nonlinear index, and I_{max} is the pulse peak intensity. Theoretical studies (*21*) also indicate that a first dip appears in the optical spectrum when ϕ_{max} reaches the value $3/2\pi$, and further dips are predicted to occur at higher values of ϕ_{max}.

These considerations can be used to estimate the width of these pulses (*21*, *22*). Referring to the spectra in Fig. 1, a pronounced dip is observed starting approximately at the bias of 0.6 A. We can then use Eq. 1 with $\phi_{max} = 3/2\pi$ and with $\Delta\omega_{rms}$ equal to the measured rms width of the spectrum at 0.6 A (250 GHz) to obtain an estimate for the pulse duration under these conditions: The result is $\tau_p = 3.2$ ps. We emphasize that this is an approximate result, primarily because it does not account for group-velocity dispersion. Finally, a pyroelectric detector was used to measure the emitted average power. The peak power of the pulses can then be estimated, given knowledge of their width and repetition rate: Values ranging from several hundreds of milliwatts to well over a watt were obtained.

Next we discuss our model and examine its supporting evidence. The proposed SML mechanism is illustrated in Fig. 3, together with a schematic cross section of the QC waveguide structure (Fig. 3A). If the nonlinear index n_2 of the laser active material is positive, the center part of the beam transverse profile, where the intensity is higher, experiences a larger refractive index relative to the edges. The resulting nonlinear dielectric waveguide increases the beam confinement near its center and hence narrows the beam diameter to an extent proportional to the optical power (*12*). This effect, which is essentially the spatial analog of self-phase modulation, is known as self-focusing or Kerr-lensing and is illustrated schematically in Fig. 3B, which refers to the waveguide lateral direction (the *x* direction in Fig. 3A). As shown, a smaller beam diameter in turn leads to a decreased mode interaction with the external gold contacts. In particular, it reduces the beam coupling to the high-loss surface plasmon mode at the metal-dielectric interface (*23*), which is a major source of waveguide losses in QC lasers (*6*). The net result is a decrease in the optical losses with increasing intensity, a so-called saturable loss mechanism, which is the fundamental ingredient for SML (*24*). In the presence of such a mechanism, it becomes favorable for the laser to emit ultrashort pulses because of their higher instantaneous intensity, and hence lower losses, relative to continuous-wave

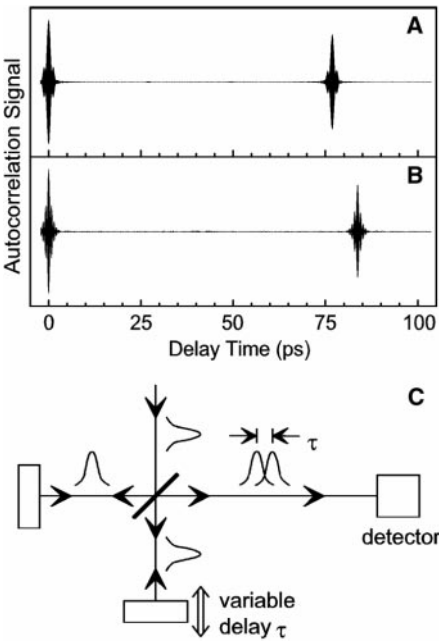

Fig. 2. Linear autocorrelation traces of two QC lasers under conditions of self–mode-locking: (**A**) a 3.5-mm-long, 8-μm wavelength device (same as in Fig. 1) at 80 K, at a bias of 1 A, and (**B**) a 3.75-mm-long, 5-μm wavelength device (from wafer D2564A) at 25 K, also at a bias of 1 A. The horizontal axis gives the delay time between the two arms of the interferometer. The time interval between consecutive spikes is the roundtrip time in the laser cavity. The side lobes observed in these spikes are due to the frequency chirp induced by self-phase modulation. (**C**) Illustration of the FTIR used to measure these traces. The constant background detected when the pulses do not overlap is automatically subtracted off the data by the FTIR.

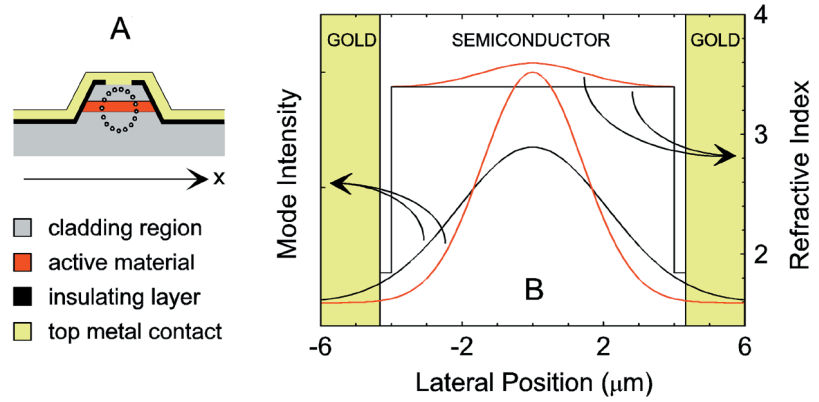

Fig. 3. (**A**) Schematic cross section of the laser waveguide structure used in this work. Typical dimensions in the lateral direction (along the *x* axis) range from 10 to 12 μm. (**B**) Refractive index profile and resulting intensity distribution of the fundamental waveguide mode along the lateral direction. Self-focusing of light occurs with increasing intensity (as in going from the black to the red curves). The same does not appreciably occur in the transverse direction (perpendicular to the active layer) because there the mode is primarily confined by the index profile of the cladding regions, consisting of several InGaAs/AlInAs(InP) epitaxial layers (*13*, *14*), where no strong nonlinearity exists.

(cw) emission, where the output energy is spread uniformly in time.

This mechanism differs in a fundamental way from previous demonstrations of SML (*1*). In the latter, the SML nonlinearity is provided by an external medium added inside the cavity or by some nonresonant transition in the laser host medium. In principle, a large "intrinsic" nonlinear refractive index is always present in any laser medium, provided by the lasing transition itself, and related to the gain coefficient through a Kramers-Kronig transformation (*24*). This is a resonant nonlinearity, involving a real population transfer across the lasing transition, so that its dynamic response is limited by the lifetime of the upper laser state. We argue that in QC lasers, because of its ultrafast lifetime and large magnitude, this intrinsic nonlinearity itself can give rise to SML. Also, we emphasize that SML by Kerr-lensing has never been previously observed in semiconductor lasers, although a similar mechanism is used with some solid-state lasers such as Ti:sapphire lasers (*3*, *25*).

All the experimental findings presented here are consistent with this picture of Kerr-lens SML. First of all, the observation of self-phase modulation confirms the existence of a large index nonlinearity, which is the fundamental ingredient of self-focusing. Furthermore, SML was only obtained in relatively long (≳3.5 mm) devices with thin (0.3 μm) dielectric blocking layers between the semiconductor material and the gold contact pads. In such devices, the saturable loss contribution resulting from self-focusing accounts for a substantial fraction of the overall losses. In particular, the thin dielectric layers allow for sufficient mode coupling to the metal, and the long waveguides ensure that such propagation losses dominate over the inevitable mirror losses [which are inversely proportional to the laser length (*24*)]. We also processed a few devices using a much thicker (4 μm) dielectric layer, and we tested a few of these devices with long waveguides, which exhibited stable cw single-mode behavior. Finally, there is no evidence of any alternative SML mechanism, such as resulting from any saturable absorber or optical feedback.

For additional evidence of SML by Kerr-lensing, we measured the far-field beam profile under cw and SML operation. In this experiment, we used an 8-μm QC laser in which SML was found to be non–self-starting. This device exhibits single-mode cw emission when dc biased; mode-locking can be achieved by modulating the current at its roundtrip frequency, as in active mode-locking (*24*). However, the laser then remains in the mode-locked state even after the modulation is switched off. This laser is ideally suited to this measurement, because it allows us to compare cw and SML cases at the same bias, temperature, and so forth. Typical results are shown in Fig. 4, where we plot collected power versus emission angle in the lateral direction. The far-field beam profile under SML conditions is broader than in cw, by more than 10%, corresponding to a narrower beam inside the waveguide. Therefore, at the higher instantaneous power levels inherent to pulsed emission, the beam does undergo self-focusing. The narrowing in beam diameter between cw and SML operation was found to increase with dc bias and hence optical intensity, also consistent with Kerr-lensing.

To estimate the corresponding loss saturation, we used an effective-index approximation (*26*) to calculate the decrease in laser losses associated with this beam narrowing. The lateral waveguide was modeled as an effective active medium (represented by the complex effective index calculated in the transverse direction) surrounded, on each side, by the dielectric blocking layer and by an effective "plasmon" medium (represented by the complex index of the plasmon mode at the gold-semiconductor interface). We used the QC waveguide parameters of (*14*), with a stripe width of 11 μm. For the nonlinear refractive index change during pulsed operation, $\Delta n = \Gamma n_2 I_{max}$, we used the value required to reproduce in this calculation the experimental beam narrowing of 10%; this is $\Delta n = 0.018$, in fair agreement with a calculation of n_2 described below. Using this value of Δn, we found a substantial decrease in the overall losses, of about 25%, qualitatively large enough to justify SML operation.

Finally, we calculated the nonlinear index of the lasing intersubband transition using the following expression (*12*), based on a two-level approximation

$$n_2 = \frac{q^2 z_{32}^2 \Delta N}{8 n_0 \varepsilon_0 h} \frac{(\Delta\nu)^2(\nu_0 - \nu)}{[(\Delta\nu/2)^2 + (\nu_0 - \nu)^2]^2} \frac{1}{I_0^{sat}}, \quad (3)$$

where z_{32} is the dipole moment of the lasing transition, ΔN is the population inversion per unit volume, n_0 is the linear refractive index, ν_0 and $\Delta\nu$ are the center frequency and the FWHM of the gain curve, I_0^{sat} is the saturation intensity at $\nu = \nu_0$, and q, ε_0, and h are the unit charge, the vacuum permittivity, and Planck's constant, respectively. Typical QC-laser parameter values (*27*) were used. Notice from Eq. 2 that n_2 is zero at the gain center frequency ν_0, which is a general property of the Kramers-Kronig transform of a symmetrical function. However, at optical frequencies detuned from ν_0 by ~100 GHz, it is already as large as $\sim 10^{-9}$ cm²/W. For comparison, this is seven orders of magnitude larger than the nonlinear index responsible for Kerr-lens SML in Ti:sapphire lasers (*3*), and it is large enough to justify the experimental findings. In fact, using Eq. 2 with $n_2 \sim 10^{-9}$ cm²/W and I_{max} estimated from typical measured average powers (~ 10 mW) gives a nonlinear phase shift ϕ_{max} on the order of a few multiples of π, consistent with the observed spectral shapes of Fig. 1. Furthermore, this calculation gives a nonlinear index change $\Delta n = \Gamma n_2 I_{max}$ of about 0.006 for the case of Fig. 4, with I_{max} estimated from the measured average power in that case (25 mW). Considering the uncertainties in the relevant physical parameters of Eq. 3, such as the homogeneous linewidth $\Delta\nu$ of the intersubband transition, and in the effective-index approximation, this is in fair agreement with the value (0.018) previously inferred from the far-field measurements of Fig. 4.

These considerations then indicate that the SML can indeed be initiated by the nonlinear index of the lasing transition itself. Finally, notice that self-focusing requires a positive value of n_2, whereas the nonlinear index of Eq. 2 is positive for $\nu < \nu_0$, but negative for $\nu > \nu_0$. The optical bandwidths observed under conditions of SML extend over several hundreds of GHz around ν_0, so that they sample both signs of n_2. However, the experimental observation of self-focusing indicates that the centers of mass of the SML spectra must lie at frequencies lower than ν_0; this was also consistently observed in our spectral

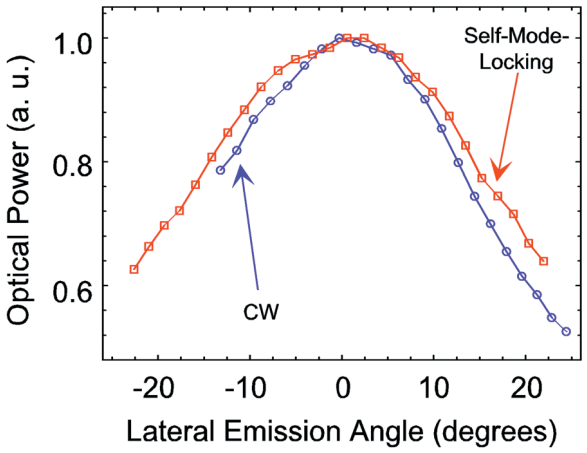

Fig. 4. Far-field beam profiles under cw and SML operation versus emission angle in the lateral direction (the *x* direction in Fig. 3A), measured from a 3.75-mm-long, 8-μm wavelength laser (from wafer D2396E) at 10 K, at a bias of 0.72 A. The two traces are superimposed to one another for ease of comparison. A relative shift of about 10° was observed between these traces.

measurements. We argue that SML is initiated by modes at these frequencies through the Kerr-lens mechanism described above; once they are locked in phase, their mutual beating produces a large enough modulation of the laser gain to bring several other modes above threshold.

References and Notes

1. W. Kaiser, Ed., *Ultrashort Laser Pulses: Generation and Applications*, vol. 60 of *Topics in Applied Physics Series* (Springer-Verlag, Berlin, 1993).
2. T. Elsaesser, J. G. Fujimoto, D. A. Wiersma, W. Zinth, Eds., *Ultrafast Phenomena XI* (Springer-Verlag, Berlin, 1998).
3. G. Steinmeyer, D. H. Sutter, L. Gallmann, N. N. Matuschek, U. Keller, *Science* **286**, 1507 (1999).
4. Present sources include mode-locked and gain-switched CO_2 lasers [see, for instance, I. V. Pogorelsky *et al.*, *IEEE J. Quantum Electron.* **31**, 556 (1995)], limited to $\lambda \simeq 10.6$ μm, and picosecond and femtosecond optical parametric oscillators [for a review, see M. H. Dunn, M. Ebrahimzadeh, *Science* **286**, 1513 (1999)], which however are still rather complex sources. Recently, we have obtained picosecond midinfrared pulses with QC lasers, including gain-switching [R. Paiella *et al.*, *Appl. Phys. Lett.* **75**, 2536 (1999)] and active mode-locking [R. Paiella *et al.*, *Appl. Phys. Lett.* **77**, 169 (2000)].
5. J. Faist *et al.*, *Science* **264**, 553 (1994).
6. F. Capasso *et al.*, *Opt. Photonics News* **10**, 31 (1999).
7. M. M. Fejer, S. J. B. Yoo, R. L. Byer, A. Harwit, J. S. Harris, *Phys. Rev. Lett.* **62**, 1041 (1989).
8. M. Segev, I. Grave', A. Yariv, *Appl. Phys. Lett.* **61**, 2403 (1992).
9. F. Capasso, C. Sirtori, A. Y. Cho, *IEEE J. Quantum Electron.* **30**, 1313 (1994).
10. E. Rosencher *et al.*, *Science* **271**, 168 (1996).
11. A. Neogi, H. Yoshida, T. Mozume, O. Wada, *J. Appl. Phys.* **85**, 3352 (1999).
12. R. W. Boyd, *Nonlinear Optics* (Academic Press, San Diego, CA, 1992).
13. J. Faist *et al.*, *IEEE J. Quantum Electron.* **34**, 336 (1998).
14. C. Gmachl *et al.*, *IEEE J. Select. Topics Quantum Electron.* **5**, 808 (1999)
15. Although room temperature operation of QC lasers is readily achieved in pulsed mode, continuous-wave operation is at present limited to temperatures below 175 K.
16. H. C. Liu, J. Li, M. Buchanan, Z. R. Wasilewski, *IEEE J. Quantum. Electron.* **32**, 1024 (1996). These detectors are also based on intersubband transitions in semiconductor quantum wells, and therefore they are very well suited for high-speed applications. The device used here has a nominal bandwidth of 12 GHz (parasitics limited).
17. For a general review of QWIPs, see B. F. Levine, *J. Appl. Phys.* **74**, R1 (1993).
18. P. R. Griffiths, J. A. de Haseth, *Fourier Transform Infrared Spectrometry* (Wiley, New York, 1986).
19. J. F. Martins-Filho, E. A. Avrutin, C. N. Ironside, J. S. Roberts, *IEEE J. Select. Topics Quantum Electron.* **1**, 539 (1995).
20. The decay in the amplitude of the spikes with increasing delay time observed in Fig. 3 is an instrumental effect, resulting from the nonperfect collimation of the beam entering the FTIR, through a mechanism known as self-apodization (*18*). This is confirmed by the fact that a decay at the same rate is observed in the interferograms for single-mode cw operation of the same lasers. On the other hand, a much faster decay would be observed if the laser modes were not phase-locked to one another (*19*).
21. G. P. Agrawal, *Nonlinear Fiber Optics* (Academic Press, San Diego, CA, 1995).
22. C. H. Lin, T. K. Gustafson, *IEEE J. Quantum Electron.* **8**, 429 (1972).
23. Surface plasmons are electromagnetic waves propagating at the interface between two materials with dielectric constants having real parts of opposite sign, such as a metal and an insulator. For more details, see, for instance, P. Yeh, *Optical Waves in Layered Media* (Wiley, New York, 1988).
24. A. Yariv, *Quantum Electronics* (Wiley, New York, 1988).
25. D. E. Spence, P. N. Kean, W. Sibbett, *Opt. Lett.* **16**, 42 (1991).
26. G. P. Agrawal, N. K. Dutta, *Long-Wavelength Semiconductor Lasers* (Van Nostrand Reinhold, New York, 1986).
27. The following parameter values, corresponding to the laser of Fig. 1, were used in the computation of $n_2{:}z_{32} = 1.9$ nm (theoretical); $\Delta\nu = 3$ THz (measured from electroluminescence spectra in similar devices); $n_0 = 3.3$ (measured from the mode separation frequency); $\Delta N = (I_{el}\tau_3)/(qV) = 8 \times 10^{15}$ cm^{-3}, with the carrier lifetime $\tau_3 = 1.5$ ps (theoretical), the volume of one period of active region $V = 677$ μm^3, at a current $I_{el} = 0.6$ A (corresponding to the second trace from top in Fig. 1); and $I_0^{sat} = (h^2\varepsilon_0 cn\Delta\nu)/(8\pi\Gamma q^2 z_{32}^2\tau_3) = 1.4$ MW/cm^2, with the active-layers confinement factor $\Gamma = 23\%$. Finally, ϕ_{max} was computed with Eq. 2 with $I_{max} = 5.5$ MW/cm^2 (inferred from the measured average power at a current of 0.6 A).

28. We thank H. Y. Hwang, A. M. Sergent, and E. Chaban for technical assistance and M. C. Wanke, R. Colombelli, and A. Tredicucci for stimulating discussions. Supported in part by Defense Advanced Research Projects Agency/U.S. Army Research Office under contract DAAD19-00-C-0096.

27 July 2000; accepted 19 October 2000

Tunable Resistance of a Carbon Nanotube–Graphite Interface

S. Paulson,[1]* A. Helser,[2] M. Buongiorno Nardelli,[3] R. M. Taylor II,[2,1] M. Falvo,[1]† R. Superfine,[1] S. Washburn[1]

The transfer of electrons from one material to another is usually described in terms of energy conservation, with no attention being paid to momentum conservation. Here we present results on the junction resistance between a carbon nanotube and a graphite substrate and show that details of momentum conservation also can change the contact resistance. By changing the angular alignment of the atomic lattices, we found that contact resistance varied by more than an order of magnitude in a controlled and reproducible fashion, indicating that momentum conservation, in addition to energy conservation, can dictate the junction resistance in graphene systems such as carbon nanotube junctions and devices.

The engineering of electronic devices relies on the control and exploitation of the electronic properties of junctions. The density of states of the two materials as a function of energy is typically used to describe these properties. New opportunities arise when the momentum transfer across the junction can be controlled. Carbon nanotubes (NTs) offer a laboratory for this control because they have a highly structured Fermi surface that restricts the allowed momentum states available at the junction (*1–3*) and have atomically smooth lattices at the contact region. The molecular size and mechanical and electronic properties of NTs have made them prime targets as components of nanometer-sized electronic and actuating devices (*4–8*). Experimental studies of devices that include both metal-NT and NT-NT junctions have demonstrated that the control of contact resistance will be essential for predictable device specifications (*9*, *10*) and that it remains an elusive goal. Here we present measurements of a multiwalled NT (MWNT) in contact with a graphite [highly oriented pyrolytic graphite (HOPG)] substrate; these materials have similar energy dispersions and available momentum states. The modulation in the electrical resistance of the contact we observed demonstrates the importance of lattice registry in NT/NT devices and opportunities for sensing and actuating device designs (*11*).

We measured the resistance of a MWNT-HOPG contact as a function of the rotation angle of the atomic lattices. Measurements were made with a two-probe technique (Fig. 1A); the HOPG substrate itself served as one lead, and a conducting atomic force microscope (AFM) tip brought into contact with the top of the NT was the other. After 200 μl of a MWNT/dichloromethane suspension was dispensed onto the rapidly spinning HOPG substrate, the sample was rinsed with ethanol, cleaned by exposure to ultraviolet light, and rinsed in water. The NT was imaged in noncontact (oscillating) mode to identify its position; then in contact mode, it was pushed, causing it to rotate (and translate) on the graphite plane until the commensurate, or in-registry, position was found, as evidenced by a sharp increase in lateral force (*12*). This position is designated as $\Phi = 0°$. Schematics of NTs in registry at $\Phi = 0°$ (Fig. 1B) and out of registry at $\Phi = 10°$ (Fig. 1C)

[1]Department of Physics and Astronomy, [2]Department of Computer Science, University of North Carolina–Chapel Hill, Chapel Hill, NC 27599, USA. [3]Department of Physics, North Carolina State University, Raleigh, NC 27695–8202, USA.

*Present address: Department of Physics and Center for Nonlinear and Complex Systems, Duke University, Durham, NC 27708, USA.

†To whom correspondence should be addressed. E-mail: falvo@physics.unc.edu